MOLECULAR IMAGING AND BIOLOGY

Mol Imaging Biol (2017) 19:183–193
DOI: 10.1007/s11307-016-0997-y

Published Online: 26 September 2016

RESEARCH ARTICLE

Comparison of Magnetic Microbubbles and Dual-modified Microbubbles Targeted to P-selectin for Imaging of Acute Endothelial Inflammation in the Abdominal Aorta

Weilan Wu,[1,2] Xuguang Feng,[2] Ye Yuan,[2] Ying Liu,[2,3] Meiyu Li,[2,3] Jianguo Bin,[2] Yunbin Xiao,[2] Wangjun Liao,[4] Yulin Liao,[2] Wenzhu Zhang,[1] Jianping Bin[2]

[1]*Department of Cardiology, Panyu Central Hospital, Guangzhou, China*
[2]*StateKey Laboratory of Organ Failure Research, Department of Cardiology, Nanfang Hospital, Southern Medical University, 1838 North Guangzhou Avenue, Guangzhou, 510515, China*
[3]*Department of Cardiology, Guangzhou Eight People's Hospital, Guangzhou, China*
[4]*Department of Oncology, Nanfang Hospital, Southern Medical University, Guangzhou, China*

Abstract

Purpose: Ultrasound molecular imaging (UMI) has potential to evaluate an inflammatory profile of endothelium. However, it is less successful in large arteries. This study compared magnetic microbubbles (MBs) selectively targeted to endothelial P-selectin and dual-targeting MBs in vitro and in vivo.

Procedures: MBs were modified with P-selectin antibody (MB_PM) or isotype control antibody (MB_CM) via a magnetic streptavidin bridge, and MBs were conjugated to P-selectin antibody (MB_P) or both P-selectin antibody and PAA-sialyl Lewis^x (MB_D) via regular streptavidin linker. Adherence of MBs was determined by using a parallel plate flow chamber at variable shear stress (0.5–24 dyn/cm^2). Adhesive and magnetic behaviors of MBs were analyzed at 4.0 dyn/cm^2 or at a flow rate of 50 mm/s. Attachment of MBs to P-selectin was determined with contrast-enhanced ultrasound (CEU) imaging of murine abdominal aorta inflammation. The expression of P-selectin was assessed by immunohistochemistry.

Results: The adhesive efficacy of MB_D was greater than MB_P and MB_CM, but lower than MB_PM under all shear stress conditions ($P < 0.05$). The behaviors of fast-binding and rolling slow down were noted in MB_D and MB_PM; meanwhile, magnetic shifting of MBs centerline was presented in MB_PM. Contrast video intensity (VI) from adhered MB_PM to P-selectin of the inflammatory aorta was significantly higher than those from MB_D and MB_P ($P < 0.05$).

Conclusions: MB_PM may be a better molecular probe than MB_D for detection of P-selectin on aorta with CEU, likely due to the shifting of axial distribution. Thus, it may improve the detection of the inflammatory profile on large arteries by UMI.

Key words: P-selectin, Ultrasound molecular imaging, Microbubbles, Inflammation

Weilan Wu and Xuguang Feng contributed equally to this work.
Electronic supplementary material The online version of this article (doi:10.1007/s11307-016-0997-y) contains supplementary material, which is available to authorized users.

Correspondence to: Wenzhu Zhang; *e-mail:* 18922238031@189.cn, Jianping Bin; *e-mail:* jianpingbin@126.com

Abbreviations: CEU, contrast-enhanced ultrasound; IL, interleukin; IOD, integrated optical density; IPP, image-pro-plus; MB_CM, microbubble with control antibody via a magnet streptavidin bridge; MB_D, microbubble with dual ligands; MB_P, microbubble with P-selection antibody; MB_PM, microbubble with P-selection antibody via a magnet streptavidin bridge; MBs, microbubbles; MF, magnetic field; MI, mechanical index; TNF, tumor necrosis factor; UMI, ultrasound molecular imaging; VI, video intensity

Introduction

Inflammation is a hallmark in the processes of numerous cardiovascular diseases [1, 2], in which the upregulation of leukocyte adhesion molecules (i.e., intercellular adhesionmolecule-1[ICAM-1] and selectins) is an essential element [3, 4]. A non-invasive and real-time clinical technique that directly assesses the status of endothelial inflammation would contribute to preclinical diagnosis and therapeutic monitoring. However, current methods are limited in vivo. Non-invasive ultrasound molecular imaging (UMI) based on contrast-enhanced ultrasound (CEU) with targeted microbubbles (MBs) is being developed to evaluate an inflammatory profile of endothelium [5–7]. Targeting strategy for MBs usually relies on specific targeting by virtue of appropriate ligands that are attached to their surface. The most often used targeting ligands on the bubble surface are monoclonal antibodies, which possess high affinity and specificity and have been shown to exhibit good targeting capability in slow and medium flow conditions ($\leq$1 dyn/cm^2) or microcirculation [8, 9]. However, these antibody-targeted MB bindings are inefficiently in large and middle-sized arteries because of the "axial flow" phenomenon [10] and high shear stress.

Several strategies for improving MB capture efficiency have been reported. For example, deformable MBs could enlarge contact area to target surface [11]; applying acoustic radiation force might concentrate and decelerate the MBs near the vessel wall [12]; the use of fast-binding selectin ligands from the sialyl Lewis group [13–15] and dual/multi-ligands [16–19] would increase the adhesion ability of MBs to activated endothelium. Encouraging studies [16, 18] have demonstrated that MBs dual-targeting to sialyl Lewis^x and ICAM-1/VCAM-1 represented greater total adhesion strength than single-targeted agents in high shear stress flow and in vitro, because sialyl Lewis^x mediating rolling could increase the chance of monoclonal antibody adhering firmly to endothelium. Nevertheless, it does not specially address the challenge of "axial flow" in large arterial vessels. Recently, our laboratory has developed a new kind of magnetic MBs which could be manipulated by a magnetic field (MF) to flow away from the centerline and slow down their motion, overcoming the two obstacles mentioned above and presenting better signal-to-noise ratio in atherosclerosis of abdominal aorta [20].

Whether the targeting efficacy of magnetic MBs could be superior to dual-targeted MBs with sialyl Lewis^x and monoclonal antibody in large arteries has not yet been demonstrated. In the current study, after developing P-selectin-targeted magnetic MBs and dual-targeted MBs with sialyl Lewis^x and P-selectin monoclonal antibody, we compared the adhesion ability of MBs to P-selectin under high shear stress conditions in vitro and hypothesized that CEU imaging by using magnetic MBs would result in more enhanced ultrasound imaging signal than that with dual-targeted contrast agents in a murine model of arterial inflammation.

Materials and Methods

The study was approved by the Animal Research Committee at the Southern Medical University and conformed to the American Heart Association Guidelines for the Use of Animals in Research.

Microbubble Preparation

Biotinylated, lipid-shelled decafluorobutane MBs were prepared by sonication as previously described [21] with the following modification. The MBs shell was conjugated to either rat anti-mouse P-selectin antibody (Becton, Dickinson and Company, MB_PM) or isotype control antibody (Becton, Dickinson and Company, MB_CM) via a magnetic streptavidin (Miltenyi Biotec) bridge. And the MBs surface was conjugated to anti-mouse P-selectin antibody (MB_P) or dual ligands (MB_D) using regular streptavidin linker. MB_D was synthesized by adding both rat anti-mouse P-selectin antibody and PAA-sialyl Lewis^x (PSLe^x, GlycoTech) to the outer shell of the same microbubbles (see Supplemental Contents, which demonstrates the preparation of MB_P and MB_D). To identify linking antibodies on the MBs under fluorescence microscope and determine the rates of ligands successfully binding to the bubble surface (ligand-binding rates) with flow cytometry, MBs with rat anti-mouse P-selectin antibody (MB_PM, MB_P, MB_D) were fluorescently labeled by FITC-goat anti-rat IgG (Jackson, American). Moreover, MB_D was also incubated with anti-sialyl Lewis^x monoclonal antibody (CD15s, Santa, American) before added rhodamine (TRITC)-goat anti-mouse IgG (Jackson, American). Fluorescent images were analyzed by image-pro-

plus (IPP, America). The size, concentration and distribution of MBs were measured by electrozone sensing (Multisizer III, Beckman Coulter, Fullerton, CA). The behavior of MBs within a magnetic field (MF) was determined as previously described [20]. To detect Additionally, using MB_CM as a control, fluorescently labeled MBs (MB_PM, MB_P, MB_D) was analyzed by quantitative flow cytometry to detect ligand-binding rates ($n = 3$).

Measurement of Microbubbles Attachment

The MB_P, MB_D, MB_CM or MB_PM (5×10^6/ml) were respectively drawn through a parallel plate flow chamber pre-coated with 200 µl of recombinant mouse P-selectin Fc chimera (1000 ng/ml, R&D, American) overnight at 4 °C at variable shear stress conditions (0.5–24 dyn/cm^2) for 10 min. Additionally, a MF-guidance was implemented for magnetic MBs for the first 5 min of infusion then removed, followed by 5 min "flush." Each flow chamber was imaged with a 20 × objective and high-resolution charge-coupled device camera (C2400, Hamamatsu Photonics, Japan). The number of adhered MBs was counted in the observed area for 60 s intervals at the 10 min time point.

Measurement of Microbubbles Detachment

These MBs (5×10^6/ml) were drawn through the flow chamber pre-coated with P-selectin with or without MF-guided and allowed to interact with the target surface by flotation at zero flow for 5 min. Subsequently, MF-guidance was removed, and these unattached MBs were immediately washed out with PBS at a lower shear stress of 0.2 dyn/cm^2. The adhered number of MBs was then counted and MBs detachment was assessed under increased shear stress every 30s.

Adhesion Behaviors of Microbubbles

In this parallel plate flow chamber assay, the processes of MBs attachment were recorded with a ×20 objective and high-resolution charge-coupled device camera as previously described. And then, the adhesion behaviors of MBs at the shear stress of 4.0 dyn/cm^2 were analyzed by set-point tracking technology of Image-Pro-Plus (IPP, America).

Flow Phantom Studies With/Without a MF-Guidance

The performance of MBs (non-magnetic and magnetic) with/without a magnet was evaluated by applying a flow phantom model that allowed direct observation of flowing MBs in a 200-µm tube. A suspension of MBs (1×10^7/ml) was drawn through the flow phantom by using an adjustable withdrawal pump (Terumo) at a fluid flow rate of 50 mm/s. Video recording were obtained by using a ×10 objective with a high-resolution charge-coupled device camera (C2400, Hamamatsu Photonics, Japan).

Model of Acute Abdominal Aorta Inflammation

Male C57BL/6 mice (20-25 g, $n = 24$) anesthetized with 1 % pentobarbital (50 mg/kg) were used to create model of acute abdominal aorta inflammation. In brief, the abdominal aorta of mice was exposed and infiltrated with cytokines (0.5 µg tumor necrosis factor (TNF)-α and 0.125 µg interleukin (IL)-1β in 0.3 ml in PBS) for 4 h. For the injection of contrast agents, a catheter was placed in the tail vein. Additionally, a group of mice ($n = 24$) untreated was served as a control.

CEU Molecular Imaging of Arterial Inflammation In vivo

A bolus of 1×10^6 MB_P, MB_D, MB_CM or MB_PM was injected into anesthetized mice randomly, and respectively, with or without a magnet (25 mm × 10 mm × 5 mm, 5000GS) placed under the abdomen. CEU molecular imaging was performed in second harmonic imaging mode (Contrast Pulse Sequencing, Sequoia, Siemen Medical Systems, Mountain View, Calif) with a centerline frequency of 7.0 MHz and mechanical index (MI = 0.18) for a duration of 15 min. The magnet was removed after the first 5 min and continuous imaging continued for 10 min. Finally, the abdominal aorta was then insonated with a high MI (1.0) for 30 s to destroy all attached immunobubbles and to immediately obtain the background images. All parameters remained constant both pre- and post-administration of MBs suspensions with or without a MF. The video was recorded and video intensities (VI) of all the abdominal aortas under different conditions were analyzed using the Yabko MCE2.7 software (University of Virginia, Charlottesville, VA).

Histopathology and Immunohistochemistry

Histological evaluation of the inflammation was systematically performed. Animals were euthanized via an overdose of pentobarbital. Abdominal aorta was excised, collected in OCT freezing medium, and frozen for histology. The traditional hematoxylin-eosin stain and the immunohistochemistry for P-selectin were performed on frozen sections of the specimens. In immunohistochemistry, rat anti-mouse CD62P (Becton, Dickinson and Company, American) or PBS was used as a primary antibody or control with a secondary anti-rat antibody (GBI, American). Slides were stained with horseradish peroxidase substrate solution (DAB + H_2O_2 prepared in distilled water) and counterstained with hematoxylin. Integrated optical density (IOD) was semi-quantified with Image-Pro Plus (IPP, $n = 10$).

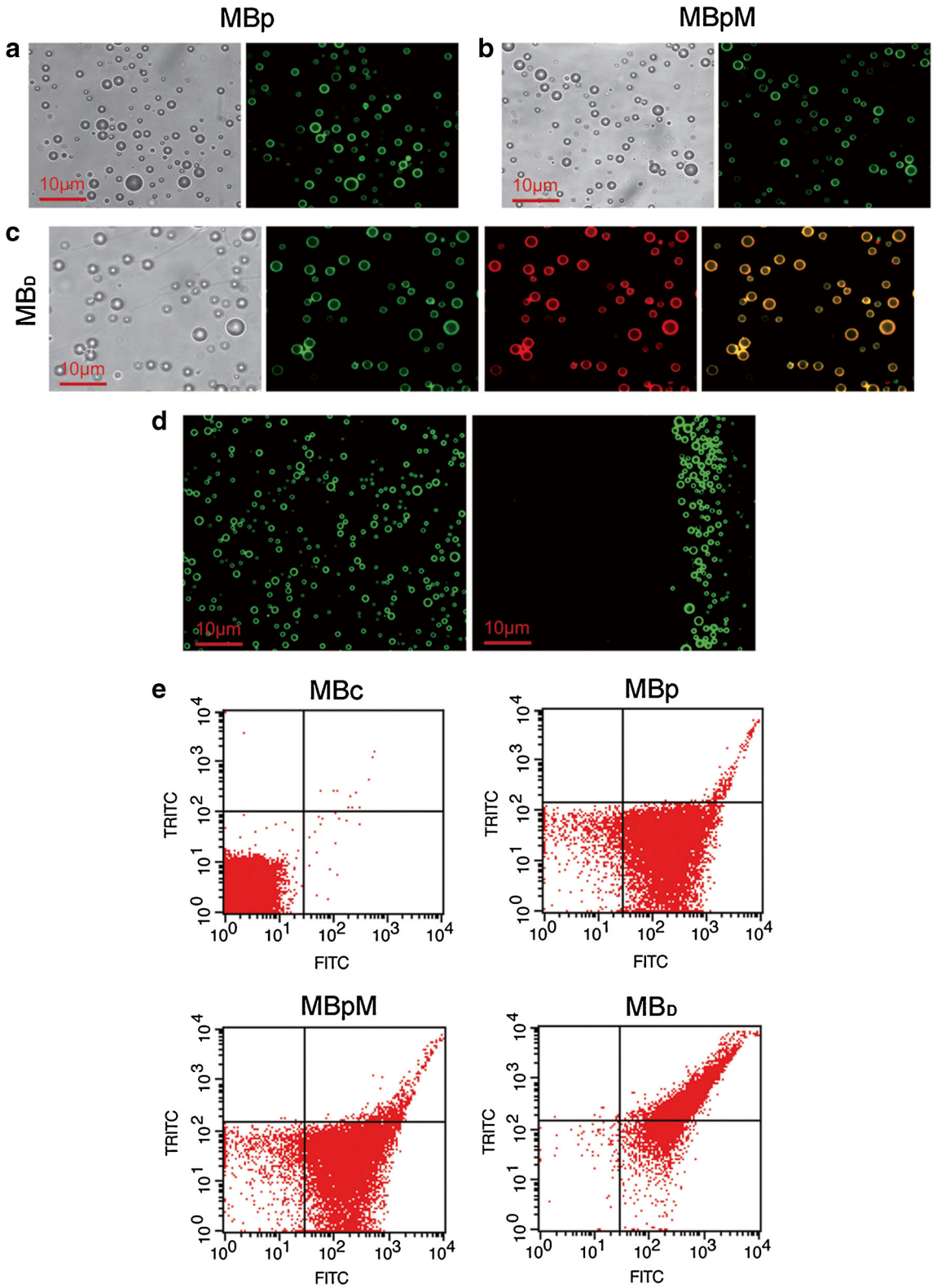

Fig. 1 Characterization of targeted microbubbles. **a**–**c** The suspension of fluorescent-labeled targeted microbubbles (MB_P, MB_PM, and MB_D) were dripped onto the microscope slide with a cover slip, and observed under optical and fluorescence microscopy. Original magnification,×200; **d** Reaction of nonmagnetic and magnetic targeted mircobubbles with fluorescence microscopy when exposed to the magnetic field; **e** Scatter diagrams from flow cytometry showed ligand-binding rates of microbubbles ($n = 3$).

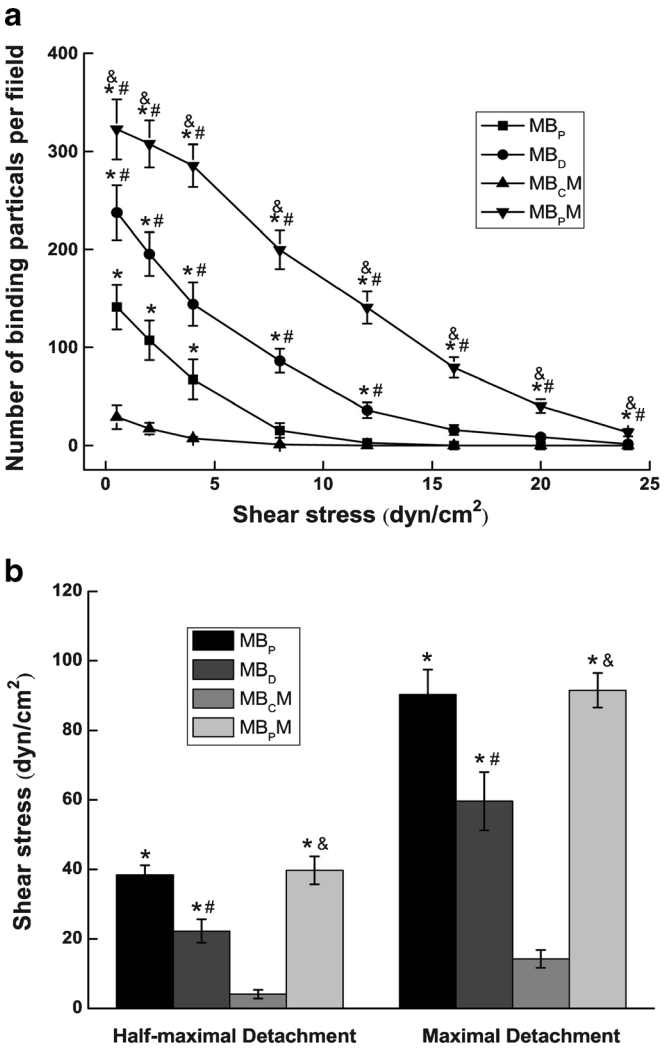

Fig. 2 Attachment and detachment effect of microbubbles. **a** The number of bound microbubbles per field at each corresponding shear stress in P-selectin-coated chamber were counted with a ×20 objective, following 10 min microbubble dispersion perfusion and buffer wash; for magnetic microbubbles, a MF-guidance was implemented for the first 5 min of infusion then removed; **b** Remaining adhered microbubbles per field were determined by increasing (set-up) shear stress at a interval of 30 s; The half-maximal and maximal detachment of microbubbles were assessed. (All mean ± SEM, $n = 6$; $^{*}P < 0.05$ from MB_CM; $^{\#}P < 0.05$ from MB_P; $^{\&}P < 0.05$ from MB_D).

Statistical Analysis

All data expressed as mean ± SEM were analyzed with SPSS software (SPSS13.0; Chicago). Factorial analysis or one-way ANOVA was applied for comparisons between groups and the Bonferroni test was performed in multiple comparisons. A value of $P < 0.05$ was considered statistically significant.

Results

Characterization of Microbubbles

The size, concentration, and distribution of MBs (MB_P, MB_D, MB_CM, MB_PM) had no significant difference between groups (all $P > 0.05$, see Supplemental Table 1). The addition of magnetic streptavidin or dual-biotinylated antibody to the bubble surface did not change the microbubble size distribution profile, indicating a lack of aggregation. Observed with fluorescence microscopy, MB_P and MB_PM emitted single green fluorescence, while MB_D gave off both green and red, presenting orange after integration by IPP (Fig. 1a–c). Additionally, magnetic MBs (MB_PM) were moved toward magnetic direction after the presence of a magnetic field, while non-magnetic MBs (MB_P) remained stationary (Fig. 1d). Fluorescently labeled ligands on the surface of MBs were analyzed by flow cytometry (Fig. 1e). The MB_P, MB_PM, and MB_D demonstrated similar ligand-binding rates (88.11 ± 1.24, 88.34 ± 1.07, and 86.46 ± 2.19 %, respectively; all $P > 0.05$).

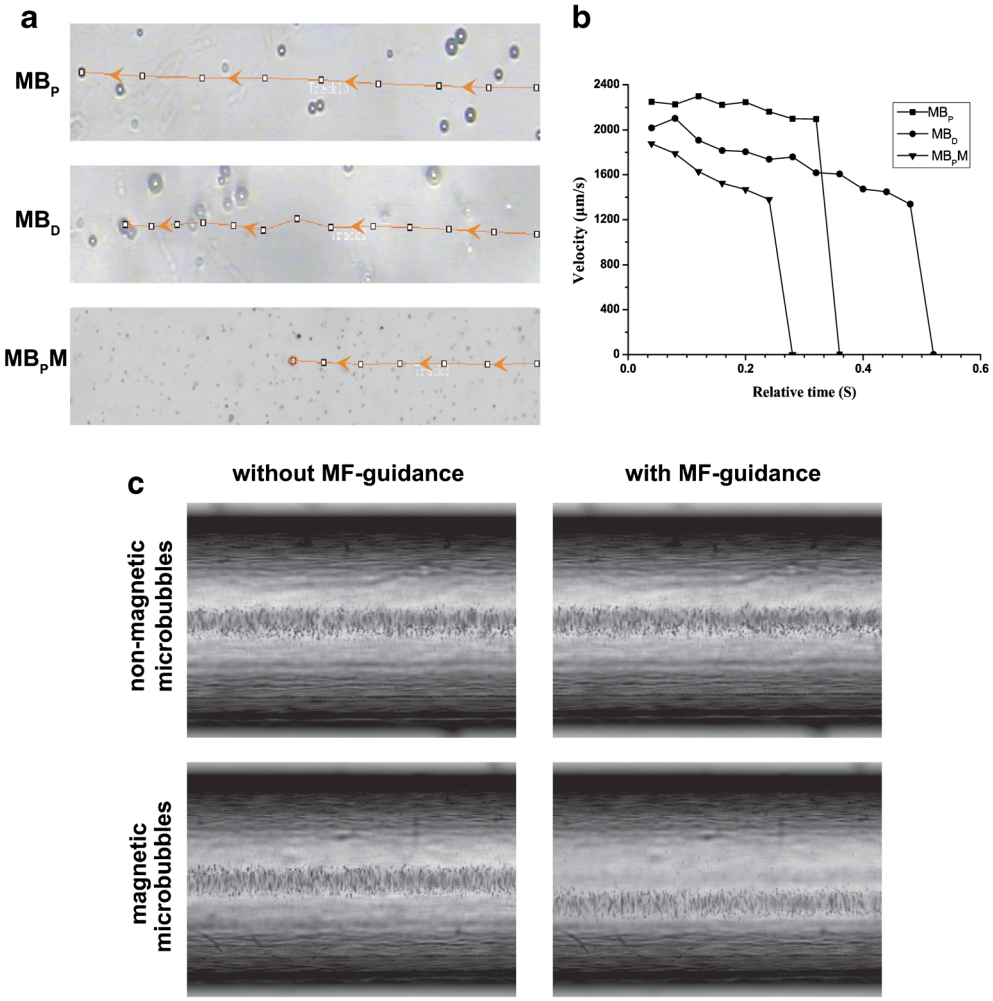

Fig. 3 Adhesion and magnetic characteristics of targeted microbubbles. **a** Rolling track of targeted microbubbles in the parallel plate flow chamber at the shear stress of 4.0 dyn/cm^2 and **b** the corresponding time-velocity curve expressed the adhesion characteristics of microbubbles. **c** Non-magnetic and magnetic microbubbles were respectively drawn through the flow phantom without/with a magnet. Changes in the lumen were recorded with a ×10 objective.

In vitro Attachment and Detachment Effect of Microbubbles

As seen in Fig. 2a, attachment of all MBs to flow chamber decreased gradually as shear stress increased. At the shear stress of 0.5, 2, 4 dyn/cm^2, MB$_P$ demonstrated significant higher attachment than MB$_C$M ($P<0.05$), while MB$_C$M had minimal attachment at the initial shear stress of 0.5 dyn/cm^2 and MB$_P$ at 8 dyn/cm^2. The adhesion number of MB$_D$ was greater than MB$_P$ and MB$_C$M, but lower than MB$_P$M at each corresponding shear stress of 0.5–16 dyn/cm^2 (all $P<0.05$). Additionally, the attachment at high shear stress (16–24 dyn/cm^2) was noted only for MB$_D$ and MB$_P$M, and the attachment number of MB$_P$M was higher than that of MB$_D$ (all $P<0.05$).

Fig. 2b showed both MB$_P$ and MB$_P$M demonstrated similar half-maximal detachment and maximal detachment (38.37 ± 2.80 and 90.40 ± 7.13 dyn/cm^2, 39.70 ± 4.02 and 91.57 ± 4.94 dyn/cm^2, respectively; $P>0.05$), which were significantly higher than those of MB$_D$ ($P<0.05$). Additionally, the half-maximal and maximal detachment of MB$_D$ were greater than both that of MB$_C$M ($P<0.05$).

Fig. 4 CEU molecular imaging of acute abdominal aorta inflammation in mice. **a** Pulsed Doppler, two-dimensional and microbubble perfusion images ensured the position of abdominal aorta and then all ultrasound molecular imaging were successfully performed. **b** Color-coded contrast enhancement of the lumen of abdominal aorta in inflammation and control mice with microbubbles; **c** The video intensity of inflammation and control with microbubbles, respectively (mean ± SEM, $n=10$). $^*P<0.05$ from MB$_C$M; $^{\#}P<0.05$ from MB$_P$; &$P<0.05$ from MB$_D$.

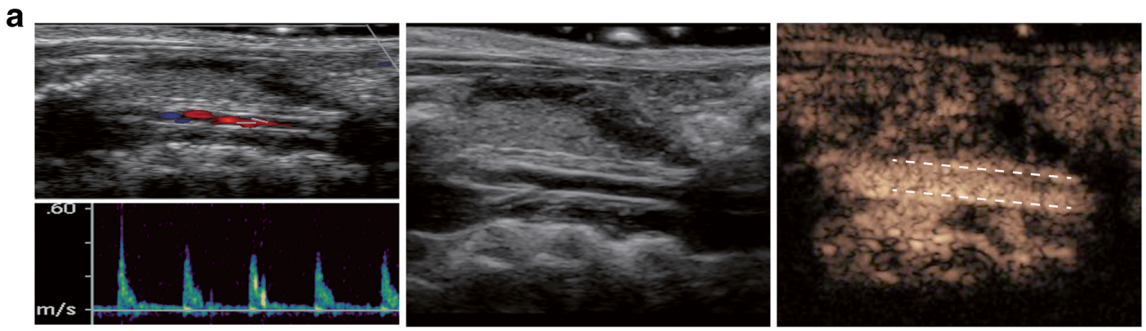
a
.60
m/s

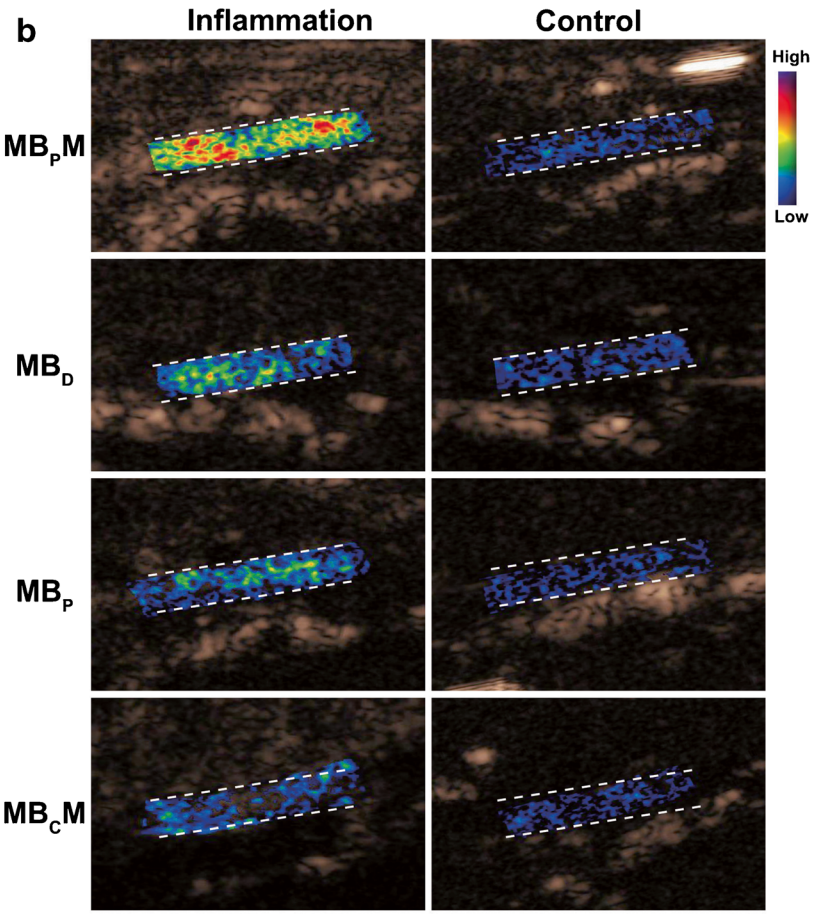
b
Inflammation
Control
High
Low
MB$_P$M
MB$_D$
MB$_P$
MB$_C$M

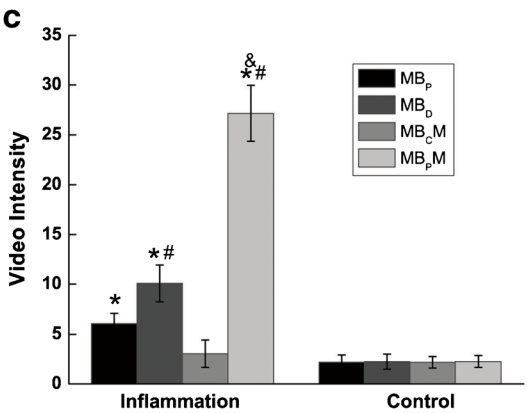
c
Video Intensity
35
30
25
20
15
10
5
0
*
*#
&
*#
MB$_P$
MB$_D$
MB$_C$M
MB$_P$M
Inflammation
Control

Adhesion and Magnetic Characteristics of Microbubbles

The rolling track of targeted MBs in the parallel plate flow chamber and the corresponding time-velocity curve was shown in Fig. 3a–b, demonstrated that MB_P was flowing at a high speed and suddenly drop to zero, while MB_D and MB_PM rolling slow down and gradually stop. As shown in Fig. 3c, non-magnetic and magnetic MBs without a magnet remain close to the axial center of the tube. And with a magnet placed under the tube, magnetic MBs flowed away from the centerline and toward magnetic direction close to the wall, while non-magnetic MBs remained the original flow.

CEU Molecular Imaging of Arterial Inflammation In vivo

All targeted CEU molecular imaging was successfully performed in abdominal aortas (Fig. 4a). As shown in Fig. 4b, background-substracted color-coded CEU images in inflammation with different MBs indicated that the greatest significant signal enhancement was observed for MB_PM, followed by MB_D, MB_P, with only minimal contrast signal from MB_CM. In control group, the four kinds of MBs expressed low and similar contrast signal. Accordingly, Fig. 4c showed that quantitative video intensity (VI) of inflammation with MB_PM was greater than that with MB_D ($P < 0.05$), and MB_D was slightly higher than MB_P ($P < 0.05$). There were no significant differences among the VI of all MBs in controls. In all cases, the CEU imaging and VI of the two animal groups with targeted MBs demonstrated great differences.

Histopathology and Immunohistochemistry

On histology, the inflammatory vessels appeared as angioedema, endothelium shriveling, and intima-media thickening compared to controls (Fig. 5a). The representative immunohistochemical staining illustrated that P-selectin was expressed abundantly in the intima and adventitia of the inflammation group, while less and seldom in the controls (Fig. 5b, c). At integrated optical density analysis, the P-selectin expression in the inflammation group was significantly higher than that in the control (Fig. 5d).

Discussion

In this study, the adhesive behaviors and ability of both site-targeted MBs were first compared at arterial shear flow conditions in vitro and in vivo after successfully development of dual-targeted MBs and single-targeted magnetic MBs to P-selectin. We found that the adhesion ability of MB_PM was superior to MB_D for targeting to P-selectin likely due to the magnetic shifting of MB_PM axial distribution, resulted in an improving visualization of the inflammatory profile in a murine model of abdominal aorta with CEU.

Several dual-targeted MBs were previously modeled based on the behavior of leukocytes during inflammation [22, 23], which use selectin ligands from the sialyl Lewis group (sialyl $Lewis^x$) and monoclonal antibodies against integrins (ICAM-1 and VCAM-1) [16, 18]. It has been known that selectin binding is fast-binding characterized by a high on-rate and off-rate, while antibody-antigen bond is firm-binding and time-consuming-binding, once formed, remained stable even at very high levels of wall shear stress [24, 25]. Thus, it has been speculated that the firm attachment of the dual-targeted MBs to the inflammatory endothelium at high wall shear stresses was mediated by antibody-antigen binding, while sialyl $Lewis^x$ promote rolling of dual-targeted MBs on the blood vessel surface to facilitate the integrins to firm adhesion. In the current in vitro study, we directly demonstrated that dual-targeted MBs with sialyl $Lewis^x$ and monoclonal antibody may offer a synergistic binding to mediate rolling and eventually attach to the blood vessel wall, similar to the behavior of leukocytes during inflammation. This finding theoretically supported the concept that the approach of dual-targeting was potentially effective in improving ultrasound contrast agents targeted to endothelial targets at high wall shear stresses, since the rolling might provide more contact time and area for antibody-based MBs to form strong bonds with target sites by antibody-antigen interactions.

In our in vivo study, the signal intensity and quantitative VI of murine abdominal aorta inflammation with MB_D were higher than with MB_P, but it was not as obvious as we expected. Ultrasound contrast MBs used as blood flow tracers exhibited rheological behavior similar to erythrocytes in vivo and, thus, tend to remain close to the axial center of blood vessels [26, 27]. This behavior and high shear stress in arteries would limit targeted MBs binding and then affect ultrasound imaging signal. Dual-targeted contrast agent emerged as a new approach [16, 18] to enhance binding efficiency and improve CEU imaging at high shear stress had been verified as we previously described. Nevertheless, the dual-targeted system did not specifically alter the axial characteristic of MBs in arteries, making the dual-targeted MBs less opportunities to contact with the target sites on the endothelium of larger arteries.

Methods to overcome the axial flow phenomenon certainly help increase the contact opportunities for MBs with target sites, thus allowing more antibody-based MBs attaching to luminal targets by firmly antibody-antigen bounds in larger vessels. One approach, developed in the past to move circulating MBs toward the vessel wall, was low-amplitude acoustic radiation [12]. But MB destruction in acoustic condition as a great deficiency limited its application and development. Recently, we have developed new magnetic MBs manipulated by a magnetic field to overcome the obstacles of the axial flow behavior in arteries

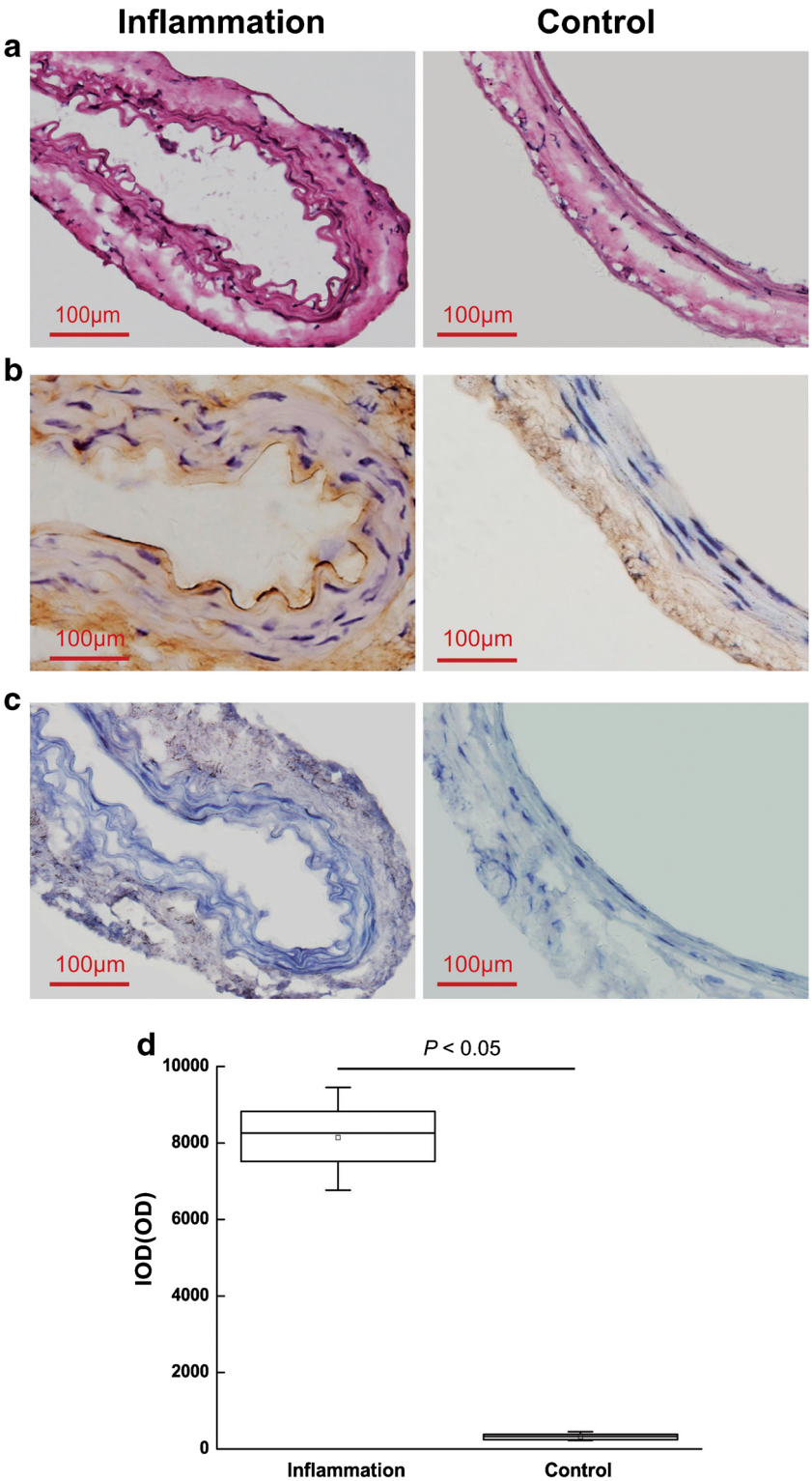

Fig. 5 Histopathology and immunohistochemistry of abdominal aorta in inflammation and control mice. **a** The lumen of inflammation but not control appeared as angioedema, endothelium shriveling and intima-media thickening in HE staining, original magnification, ×400; **b**–**c** Corresponding expression of P-selectin in inflammation and control abdominal aorta was observed by immunohistochemistry. The primary antibody was substituted by PBS as a negative control (**c**), original magnification, ×400; **d** Box plot of P-selectin staining according to integrated optical density (IOD), determined with software in the both groups (mean ± SEM, $n = 10$), showed greater P-selectin staining in the inflammation group.

[20]. In vitro, we presented that magnetic MBs could move toward magnetic direction and then flow away from the centerline to the wall, allowing greater contact with the substrate in a short time and more opportunities for microbubble-target interaction. And the adhesion behavior of magnetic targeted MBs showed fast-binding and rolling slow down, providing more time to form strong and permanent bond pairs that will prevent subsequent dislodgement. Therefore, the new magnetic MBs would have better targeting efficacy than dual-targeted MBs, which had not yet been reported.

In this study, parallel plate flow chamber assays in vitro clearly demonstrated that the binding of magnetic MBs to the substrate surface was significantly higher than that of dual-targeted MBs at each corresponding shear stress of 0.5–24 dyn/cm^2. In vivo, targeted imaging of arterial inflammation was successful using magnetic or dual-targeted MBs with CEU, while the magnetic MBs presented stronger ultrasound imaging signal and higher quantitative VI than dual-targeted MBs as we expected. These findings manifested that magnetic MBs possess better targeting efficacy than dual-targeted MBs even under high shear flow conditions in vitro and in vivo. The magnetic MBs system could manipulate the axial distribution and motion speed of MBs, providing more opportunities for MBs to contact with target sites, and more time for MBs to form more permanent bond pairs that will prevent subsequent dislodgement. Indeed, the dual-targeted MBs could increase the time of antibody-antigen interactions by faster-binding ligands, thus improving microbubble binding to luminal targets at high wall shear stresses. However, dual-targeted MBs do not specifically change the axial flow behavior of MBs.

The following limitations of this study need to be addressed. The magnetic force was placed steadily and specifically under the abdominal aorta, and the field strength was not able to be adjusted to optimize the system for optimal effect. For clinical applications, future studies will need to detect the effects of a rotating magnetic field with field gradient strength scaled up, although high field gradient electromagnets has been already available in magnetic drug targeting in pigs [28, 29]. Additionally, flow through the perfusion chamber was non-pulsatile and included no blood components. It has been reported that the "diastolic" phase between pulses and the presence of numerous blood cells may promote adhesion and enhance binding [7, 30]. While sialyl Lewis^x as a natural blood group antigen can be applied in a wide variety of animal species, the biotin-streptavidin bridge should be replaced in clinical applications. Alternative methods exist for direct covalent conjugation of ligands to the microbubble shell. To compare the adhesion of dual-targeted MBs and single-targeted magnetic MBs better in vitro, the dual-targeted MBs rely on selectin expression only. MB_D dual-targeting to both P-selectin antibody and PAA-sialyl Lewis^x was confirmed with indirect methods and lack of direct experiments.

Conclusion

MB_PM is superior to MB_D for targeting to P-selectin of endothelial inflammation in large arteries, since the axial distribution and motion speed ofMB_PM could be manipulated with a magnetic field. It might improve the detection of the inflammatory profile on large arteries with CEU.

Acknowledgments. Dr Wu and Dr Feng designed the study, collected and interpreted the data, and wrote the report under the supervision and correction of Dr Zhang and Dr Bin as senior authors. Dr Xiao carried out the statistical analysis, while Drs Liu, Yuan, Li and Bin interpreted the data and contributed to the writing of the report. Drs Liao was involved in drafting the report and reviewing it critically for important intellectual content. Dr Wu and Dr Bin are responsible for the overall content and take responsibility for the final submission.

Compliance with Ethical Standards

Conflict of Interest

The authors declare that they have no conflict of interest.

References

1. Epstein FH, Ross R (1999) Atherosclerosis—an inflammatory disease. N Engl J Med 340:115–126
2. Tanaka H, Sukhova GK, Swanson SJ et al (1994) Endothelial and smooth muscle cells express leukocyte adhesion molecules heterogeneously during acute rejection of rabbit cardiac allografts. Am J Pathol 144:938
3. Cybulsky MI, Gimbrone M (1991) Endothelial expression of a mononuclear leukocyte adhesion molecule during atherogenesis. Science 251:788–791
4. Nakashima Y, Raines EW, Plump AS et al (1998) Upregulation of VCAM-1 and ICAM-1 at atherosclerosis-prone sites on the endothelium in the ApoE-deficient mouse. Arterioscler Thromb Vasc Bio 18:842–851
5. Lindner JR, Song J, Christiansen J et al (2001) Ultrasound assessment of inflammation and renal tissue injury with microbubbles targeted to P-selectin. Circulation 104:2107–2112
6. Weller GE, Villanueva FS, Klibanov AL et al (2002) Modulating targeted adhesion of an ultrasound contrast agent to dysfunctional endothelium. Ann Biomed Eng 30:1012–1019
7. Kaufmann BA, Sanders JM, Davis C et al (2007) Molecular imaging of inflammation in atherosclerosis with targeted ultrasound detection of vascular cell adhesion molecule-1. Circulation 116:276–284
8. Takalkar AM, Klibanov AL, Rychak JJ et al (2004) Binding and detachment dynamics of microbubbles targeted to P-selectin under controlled shear flow. J Control Release 96:473–482
9. Klibanov A, Rychak J, Yang W et al (2006) Targeted ultrasound contrast agent for molecular imaging of inflammation in high-shear flow. Contrast Media Mol I 1:259–266
10. Keller MW, Segal SS, Kaul S et al (1989) The behavior of sonicated albumin microbubbles within the microcirculation: a basis for their use during myocardial contrast echocardiography. Circ Res 65:458–467
11. Rychak JJ, Lindner JR, Ley K et al (2006) Deformable gas-filled microbubbles targeted to P-selectin. J Control Release 114:288–299
12. Dayton P, Klibanov A, Brandenburger G et al (1999) Acoustic radiation force in vivo: a mechanism to assist targeting of microbubbles. Ultrasound Med Biol 25:1195–1201
13. Klibanov AL (2007) Ultrasound molecular imaging with targeted microbubble contrast agents. J Nucl Cardiol 14:876–884
14. Rychak J, Li B, Acton S et al (2006) Selectin ligands promote ultrasound contrast agent adhesion under shear flow. Mol Pharm 3:516–524
15. Klibanov AL (2006) Microbubble contrast agents: targeted ultrasound imaging and ultrasound-assisted drug-delivery applications. Invest Radiol 41:354–362
16. Weller GE, Villanueva FS, Tom EM et al (2005) Targeted ultrasound contrast agents: In vitro assessment of endothelial dysfunction and multi-targeting to ICAM-1 and sialyl Lewisx. Biotechnol Bioeng 92:780–788

17. Ferrante E, Pickard J, Rychak J et al (2009) Dual targeting improves microbubble contrast agent adhesion to VCAM-1 and P-selectin under flow. J Control Release 140:100–107
18. Cho Y-K, Yang W, Harry BL, et al. (2006) Dual-targeted contrast enhanced ultrasound imaging of atherosclerosis in apolipoprotein e gene knockout mice. Circulation 114: II_759.
19. Willmann JK, Lutz AM, Paulmurugan R et al (2008) Dual-targeted contrast agent for US assessment of tumor angiogenesis in vivo 1. Radiology 248:936–944
20. Wu J, Leong-Poi H, Bin J et al (2011) Efficacy of contrast-enhanced US and magnetic microbubbles targeted to vascular cell adhesion molecule–1 for molecular imaging of atherosclerosis. Radiology 260:463–471
21. Bin J, Yan Y, Yang L et al (2009) Evaluation of ICAM-1 expression for a recent myocardial ischemia in late time window with ultrasound molecular imaging. Circulation 120:S326
22. Ebnet K, Vestweber D (1999) Molecular mechanisms that control leukocyte extravasation: the selectins and the chemokines. Histochem Cell Biol 112:1–23
23. Springer TA (1994) Traffic signals for lymphocyte recirculation and leukocyte emigration: the multistep paradigm. Cell 76:301–314
24. Eniola AO, Willcox PJ, Hammer DA (2003) Interplay between rolling and firm adhesion elucidated with a cell-free system engineered with two distinct receptor-ligand pairs. Biophys J 85:2720–2731
25. Bhatia SK, King MR, Hammer DA (2003) The state diagram for cell adhesion mediated by two receptors. Biophys J 84:2671–2690
26. Lindner JR, Song J, Jayaweera AR et al (2002) Microvascular rheology of definity microbubbles after intra-arterial and intravenous administration. J Am Soc Echocardiog 15:396–403
27. Ismail S, Jayaweera AR, Camarano G et al (1996) Relation between air-filled albumin microbubble and red blood cell rheology in the human myocardium. Influence of echocardiographic systems and chest wall attenuation. Circulation 94:445–451
28. Gleich B, Hellwig N, Bridell H et al (2007) Design and evaluation of magnetic fields for nanoparticle drug targeting in cancer. Ieee T Nanotechnol 6:164–170
29. Alexiou C, Diehl D, Henninger P et al (2006) A high field gradient magnet for magnetic drug targeting. Ieee T Appl Supercon 16:1527–1530
30. King MR, Hammer DA (2001) Multiparticle adhesive dynamics. Interactions between stably rolling cells. Biophys J 81:799–813